Heparan sulfate co-immobilized with cRGD ligands and BMP2 on biomimetic platforms promotes BMP2-me diate d osteogenic differentiation

Julius Sefkow-Werner, Paul Machillot, Adrià Sales, Elaine Castro-Ramirez, Melissa Degardin, Didier Boturyn, Elisabetta Ada Cavalcanti-Adam, Corinne Albiges-Rizo, Catherine Picart, Elisa Migliorini

TITLE:

Heparan sulfate co-immobilized with cRGD ligands and BMP2 on biomimetic platforms promotes BMP2-mediated osteogenic differentiation

Julius Sefkow-Werner[1,2], Paul Machillot[1,2], Adria Sales[1,2], Elaine Castro-Ramirez[1,2], Melissa Degardin[3], Didier Boturyn[3], Elisabetta Ada Cavalcanti-Adam[4], Corinne Albiges-Rizo[5], Catherine Picart[1,2,6]*, Elisa Migliorini[1,2]*

[1] Grenoble Institute of Technology, Université Grenoble Alpes, LMGP UMR 5628, Grenoble, France

[2] CEA, CNRS, UGA, BRM ERL 5000, Grenoble, France

[3] Université Grenoble Alpes, CNRS, DCM, Grenoble, France

[4] University of Heidelberg, Department of Biophysical Chemistry, Heidelberg, Germany

[5] Institut Albert Bonniot, Université Grenoble Alpes, INSERM U1209, CNRS UMR5309, Grenoble, France

[6] CEA, direction of fundamental research, interdisciplinary research institute of Grenoble (IRIG), FRE CNRS

* co-corresponding authors

Elisa Migliorini, 3 parvis L. NEEL 38016 GRENOBLE
Tel: (33)-04 56 52 93 24 Email: elisa.migliorini@grenoble-inp.fr
Catherine Picart, 17 rue des Martyrs, 38016 GRENOBLE
Email: catherine.picart@cea.fr

KEYWORDS: biomimetic approach, BMP2, heparan sulfate, integrins, osteogenic differentiation, cell adhesion

ABSTRACT

The chemical and physical properties of the extracellular matrix (ECM) are known to be fundamental for regulating growth factor bioactivity. The role of heparan sulfate (HS), a glycosaminoglycan, and of cell adhesion proteins (containing the cyclic RGD (cRGD) ligands) on bone morphogenetic protein 2 (BMP2)-mediated osteogenic differentiation has not been fully explored. In particular, it is not known whether and how their effects can be potentiated when they are presented in controlled close proximity, as in the ECM. Here, we developed streptavidin platforms to mimic selective aspects of the *in vivo* presentation of cRGD, HS and BMP2, with a nanoscale-control of their surface density and orientation to study cell adhesion and osteogenic differentiation. We showed that whereas a controlled increase in cRGD surface concentration upregulated BMP2 signaling due to β_3 integrin recruitment, silencing both β_1 and β_3 integrins negatively affected BMP2-mediated phosphorylation of SMAD1/5/9 and alkaline phosphatase expression. Furthermore, the presence of adsorbed BMP2 promoted cellular adhesion at very low cRGD concentrations. Finally, we proved that HS co-immobilized with cRGD both sustained BMP2 signaling and enhanced osteogenic differentiation compared to BMP2 directly immobilized on streptavidin, even with a low cRGD surface concentration. Altogether, our results show that HS facilitated and sustained the synergy between BMP2 and integrin pathways and that the co-immobilization of HS and cRGD peptides optimised BMP2-mediated osteogenic differentiation.

1. INTRODUCTION

The chemical and physical properties of the extracellular matrix (ECM) as the main regulator of processes such as cellular proliferation, migration, adhesion, differentiation and tissue formation have been widely explored [1, 2]. Today, the role of glycosaminoglycans (GAGs) in the preservation, presentation and activation of extracellular components has become an important area for research [3-6]. One of the roles of the extracellular components is to regulate the activity of growth factors (GFs) such as the broadly-studied bone morphogenetic protein 2 (BMP2), known for its osteogenic potential [7] and its clinical use in *de novo* bone formation. BMP2 binds mainly to the BMP2 cell receptor complex formed by the transmembrane BMP receptor type I and BMP receptor type II. This triggers the phosphorylation of SMAD1/5/8 and, together with SMAD 4, it translocates to the nucleus [8] to activate transcription of target genes. BMP2 upregulates transcription factors such as Osterix or Runx2, both of which are markers for osteogenic differentiation. It also activates the SMAD-independent osteogenic signaling cascade which leads to alkaline phosphatase expression (ALP) [9, 10].

In vivo, BMP2 most likely does not present alone in solution, but rather bound to extracellular matrix (ECM) components, such as the GAG, heparan sulfate (HS) [11-13], and fibronectin [14]. It is generally accepted that

this binding protects GFs from degradation and modulates their availability to their receptors in the cell membrane [15-17].

Simplified biomimetic model systems can be used to understand this complex system. They make it possible to assemble individual components of the cell's natural environment to reveal their specific role.

In the osteogenic context, various approaches have been reviewed recently [18, 19], all focusing on presenting GFs *via* ECM molecules such as proteins and GAGs. For example, polyelectrolyte multilayer films can be engineered with tunable stiffness [20] and trap BMP2 with high affinity [21, 22]. To study the isolated or combined effect of single ECM components on cells, versatile surfaces with precise control of molecular orientation and surface density are needed. We previously developed streptavidin (SAv) platforms to study the molecular role of GAGs on GF binding [23, 24] and short-term cellular responses [25, 26]. Gold-sputtered glass surfaces were functionalized with a self-assembled monolayer of biotinylated PEG-thiol on which SAv formed a second monolayer, thus offering free highly specific biotin binding sites. On these platforms, HS was immobilized *via* its reducing end, which mimics its attachment to core proteins on HS proteoglycans [27]. BMP2 binding to iHS was studied at the molecular level [28].

The effect of HS on BMP2 signaling is the subject of scientific debate [13, 29-33]. It was previously shown that HS inhibits BMP2 bioactivity [31-35] as it does for different GFs [36]. But results from our group suggest that exogenous HS in particular has a positive effect on BMP2 bioactivity compared to immobilized BMP2 (iBMP2) [28], partially in line with previous observations on BMP2 bound to soluble HS in cell media [13]. However, insufficient cellular adhesion has prevented additional studies of the effect of immobilized HS on later effectors of the BMP2 signaling cascade and therefore a clear readout on how extracellular HS can influence BMP2 bioactivity through osteogenic differentiation.

To tune the bioactivity of BMP2 by HS and to improve its use for regenerative medicine applications, it is also important to further understand the influence of ECM adhesion proteins [37, 38] on BMP2-mediated osteogenic differentiation. In recent years, the interplay between integrins and GF receptors has been the topic of several studies [38-41], but it remains to be proved and quantified on the same biomaterial whether this crosstalk is bidirectional, in particular regarding integrins and BMP receptors.

Integrins are transmembrane receptors consisting of α and β subunits which bind to cell adhesion ligands in the ECM [42] and allow cells to spread by developing focal adhesions. It has been shown that surface-presented BMP2 can induce cell spreading on soft films, whereas cells did not spread on soft films devoid of BMP2 [43]. In this particular context, β_3-integrins are needed for BMP2-induced cell spreading and to control SMAD 1/5/8 phosphorylation and degradation. However, the type of integrins involved in growth factor signaling might be context dependent. Experiments with vascular endothelial growth factor (VEGF) have

shown that β_1-integrins upregulate VEGF-induced vascularization in hydrogels, while β_3-integrins have no influence [44]. It has further been demonstrated on mesenchymal stem cells that increased lateral spacing of arginine-glycine-aspartic acid (RGD) containing peptide ligands significantly decreases alkaline phosphatase (ALP) activity and reveals a similar trend on Runx2 expression [45]. *In vivo* studies with Drosophila have revealed that integrins are also necessary for a peak p-SMAD1/5/9 signal [40]. Collagen IV mutant embryos presented a reduced p-Mad (the equivalent of p-SMAD) signaling.

How HS is able to contribute to BMP2-mediated signaling and osteogenic differentiation, as well as interfere with the cooperation between BMPRs and integrins, is still an open question.

Here, we studied the influence of integrin activation and the additional role of HS on BMP2-mediated signaling with a well-defined biomimetic SAv platform. These platforms co-presented cyclic RGD peptides (cRGD) known to bind and activate integrins such as β_1 and β_3 subunits [46] and immobilized and oriented HS (iHS). The cyclic arginine-beta alanine-aspartic acid (cRβAD here named cRAD) peptide was adopted as the negative control as it has a significantly lower affinity for integrins [46]. BMP2 was presented either immobilized or adsorbed to iHS with the same surface density. Cellular responses were assessed by quantifying cell adhesion and cell osteogenic differentiation at early and later stages. To this end, we selected two relevant cell types that are BMP2-responsive: C2C12 murine myoblasts [47] and human periosteum-derived stem cells (hPDSCs) that are currently investigated for their bone regenerative capacities [48]. To gain insight into the role of β_1 and β_3 integrins on early and late BMP2-mediated signaling, we performed knock-down experiments by silencing these receptors.

2. EXPERIMENTAL PROCEDURES

2.1 *Buffers, heparan sulfate and proteins*

10 mM Hepes (Fisher, Illkirch, France) at pH 7.2 was used as the working buffer for surface functionalization, for all quartz-crystal microbalance with dissipation monitoring (QCM-D) and spectroscopic ellipsometry (SE) measurements. Filtered phosphate buffered saline (PBS, Dublbecco's without $MgCl_2$ and $CaCl_2$, Sigma-Aldrich) was applied in all the working steps related to the cells.

HS derived from porcine intestinal mucosa [49] (Celsus Laboratories, Cincinnati, OH, USA) was conjugated with biotin as previously described [24]. Human recombinant BMP2 (26 kDa, homodimer), from a Chinese hamster cell line, was purchased from R&D Systems Inc. (Minneapolis, MN, USA). BMP2 was biotinylated by NHS-ester coupling using EZ-Link® NHS-PEG12-Biotin 5.6 nm long (Thermo Scientific, Rockford, IL, USA) as described in [28]. Lyophilized SAv, (53 kDa) and ATTO 565-Biotin (921 DA, bATTO) were purchased from Sigma-Aldrich. Biotinylated cRGD and cRAD (3.9 and 4.2 kDa, respectively) were obtained by amide-coupling

PEG (~ 3.2 kDa), with a biotin at one end and an activated acid group at the other (b-PEG-NHS, Sigma-Aldrich), to a cyclic RGD pentapeptide c(-RGDfK) (GenScript Biotech, Netherlands) or cyclic RAD (RβAD, synthesized in the lab of Dr Didier Boturyn), at the lysine side-chain as written in [26]. Thawed protein solutions were used within a week and further diluted (**Table 1**).

2.2 Sensors and surface preparation

Gold-coated QCM-D sensors (QSX301) from Biolin Scientific (Västra Frölunda, Sweden) and gold-sputtered glass cover slips (24 × 24 mm; Menzel Gläser, Braunschweig, Germany) for cellular studies were immersed in 1 mM of PEG disulfide and biotinylated PEG thiol (Polypure, Oslo, Norway) at a molar ratio of thiol equivalents of 95:5 in ethanol to build a monolayer.

For Western blot and qPCR experiments that demand large quantities of the sample, whole surfaces were then placed in a UV-sterilized plastic dish. When samples were prepared for automated imaging with standardized 96-well plates, gold-coated surfaces were attached *via* double-sided adhesive tape (FRAP Sandwich set, Paul Marienfeld GmbH, Lauda-Koenigshofen, Germany) to the bottom side of a UV-sterilized bottom-less 96-well plate (Greiner bio-one, Kremsmünster, Austria), separating 1 surface into 4 wells.

2.3 Assembly of biomimetic platforms

The QCM-D sensors were functionalized step-by-step *in situ* tracked by QCM-D or SE as previously reported [28]. Biomimetic platforms were functionalized *ex situ,* incubating molecules at the desired concentration under sterile conditions. To prepare co-functionalized platforms, the following concentrations and incubation times were used:

Table 1: Molecule concentrations and incubation times.

Molecule	*Concentration (μM)*	*Incubation time (min)*
*Streptavidin (**SAv**)*	0.17	30
*Biotinylated cyclic Arginylglycylaspartic acid (**cRGD**)*	0.14	4 (partially saturated) or 10 (saturated)
***cRGD-PEG** mixture*	0.25	3 (partially saturated)
*Biotinylated cyclic Arginylalanineaspartic acid (**cRAD**)*	0.24	4 (partially saturated)
*Biotinylated Atto 565 (**bATTO**)*	11	20
*Biotinylated Heparan sulfate (**iHS**)*	0.83	30
*Biotinylated bone morphogenetic protein 2 (**iBMP2**)*	9.6×10^{-2}	60
*Adsorbed BMP-2 (**aBMP2**)*	9.6×10^{-2}	90
*Soluble BMP-2 (**sBMP2**)*	6×10^{-3}	

The concentrations and time of incubation of cRGD and cRAD were chosen in a way to obtain the desired sub-monolayer surface density which then makes possible the subsequent binding of iHS or iBMP2. Soluble BMP2 (sBMP2) at a concentration of 6 nM was always added into the cell media at the moment when cells were plated on the corresponding condition. The quantity of soluble BMP2 in the media largely corresponds

to the amount of either aBMP2 or iBMP2 on the platform surface. The wells of 96-well plates and large round surfaces with surface areas of 35 mm^2 and 450 mm^2 respectively therefore had 8.6 ng and 110 ng of iBMP2 or 10.4 ng and 134 ng of aBMP2 on the surface (see **Table 2**). 100 µl of cell media per well and 1 ml of cell media on round surfaces carry 10 ng and 100 ng of sBMP2 respectively. We point out that a direct comparison of sBMP2 and surface-bound BMP2 lags due to the disparity in its dorsal and ventral presentation to the cell.

2.4 Quartz crystal microbalance with dissipation monitoring (QCM-D) and spectroscopic ellipsometry (SE)

QCMD and SE where used to characterize molecule binding events on the SAv monolayer to deduce binding kinetics and areal mass density respectively and was previously described in detail [25, 50, 51]. All surface functionalization steps were carried out *in situ* using the concentrations and incubation time indicated in **Table 1**.

2.5 Cellular culture

Mouse C2C12 myoblasts (CRL-1772, ATCC, USA) and human periosteum-derived stem cells (hPDSCs, kindly provided by Prof. Franck Luyten, Leuven, Belgium) [48, 52, 53], were used for the functional assays. Both cell types were cultured in typical tissue-treated polystyrene cell culture flasks or Petri dishes as sub-confluent monolayers in growth medium consisting of Dulbecco's modified Eagle's medium (DMEM) (Gibco) supplemented with heat-inactivated fetal bovine serum (FBS, 10 %) (FBS, PAA Laboratories, Toronto, Canada) and antibiotic-antimycotic (1 %, Gibco) at 37 °C and 5 % CO_2 until a passage number of less than 12. hPDSCs (< 9 passages) were cultured as previously described [52] in high-glucose Dulbecco's modified medium, supplemented with 10% fetal bovine serum and 1% antibiotic-antimycotic.

Both C2C12 and hPDSCs were always serum-starved 4 hours prior to plating on the biomimetic platforms. Accutase (Sigma Aldrich) was used to detach cells from culture flasks prior to the experiment in DMEM without FBS supplement. Functionalized surfaces with plated cells were always incubated at 37 °C, 5% CO_2 with media (0% FBS) if not specified otherwise.

2.6 Knock-down of integrins

To silence integrins on C2C12 cells, we used a protocol optimized in our group [43]. Briefly, C2C12 were transfected twice, 48 h and 24 h before starving and then plating on the surfaces. The transfection mix consisted of lipofectamine RNAiMAX (Invitrogen, Carlsbad, Ca, USA) diluted in Opti-MEM medium (Gibco) which was gently mixed with 100 µM Silencing RNA for β_1-, β_3-integrin (ON-TARGET plus SMART pool SiRNA, Dharmacon, UK) or scrambled silencing RNA (ON-TARGET plus non-targeting siRNA, Dharmacon, UK). This mix was added drop by drop into plastic plates and repeated 24 h later to ensure successful transfection. The moment cells were plated on functionalized surfaces, no more silencing RNA was added to the fresh media.

2.7 Cell adhesion and differentiation for microscopy analysis

For live cell imaging used to quantify cell numbers, 30 000 starved cells for each condition were plated on functionalized 96-well plates and incubated for 45 minutes (C2C12 cells) or 1h and 45 minutes (hPDSCs). Nuclei were stained 30 min after plating with 10 ng/mL Hoechst (Invitrogen) in PBS. 15 min later, images were taken on eight defined positions with the Zeiss Axio Observer 7 epifluorescence microscope (Carl Zeiss Sas, Le Pecq, France) with the cell culture environment (37 °C, 5 % CO_2) provided by the heating unit XL S (Zeiss). After rinsing carefully 4 times with 100 µL PBS to remove non-adherent cells, fluorescent images (Colibri 7, 385 nm, 21 % intensity) were taken again with the 20x objective at the same positions to quantify the percentage of adhering cells. 30 minutes after rinsing, the cells were fixed with PFA 4% (Sigma-Aldrich) for 20 min.

To measure C2C12 cell area and p-SMAD1/5/9 translocated to the nucleus [54], 10 000 starved cells per condition were plated on functionalized 96-well plates and fixed after 1.5 hours by rinsing 3 times with 100 µL PBS before adding 100 µL PFA fixation.

To quantify p-SMAD1/5/9 via immunofluorescence we adapted existing protocols already published [26, 54, 55]. Fixed cells were first permeabilized with 0.2% Triton X-100 (Sigma-Aldrich) (w/v) in PBS for 3 min and blocked for 1h with 3% BSA (Sigma-Aldrich) at RT. Primary rabbit anti-p-SMAD1/5/9 (Cell Signaling Technology, Danvers, Ma, USA) was diluted 1:400 and for staining, F-actin Phalloidin-Rhodamine (Sigma-Aldrich) was used at a dilution of 1:1000. For β_1- (rat anti-integrin β_1, MAB 1997, Millipore, Darmstast, Germany 1:100) and β_3-integrins (rat anti-mouse integrin β_3, Luc-A5, emfret Analytics, Würzburg, Germany 1:100) no Triton treatment was used. All primary antibodies were incubated overnight at 4 °C diluted in PBS with 3% BSA. Secondary antibodies (goat anti-rat/rabbit Alexa Fluor 488, Thermo Fischer Scientific), as well as F-actin and DAPI, were incubated for 90 min at RT in PBS and 3% BSA. As a final step, a solution of 2.5% w/v Dapco (Sigma-Aldrich) in PBS at pH=7.8 preserved the fluorescence activity.

For highly magnified images to visualize β_1- and β_3-integrins together with F-actin and the nucleus, a 63x oil-immersed lens (Plan-Apochromat 63x/1,4 Oil DIC, Carl Zeiss Sas, Le Pecq, France) from a Zeiss LSM 700 confocal microscope (Carl Zeiss Sas) was used. Cell area and p-SMAD1/5/9 were simultaneously studied by capturing p-SMAD1/5/9, F-actin and DAPI signals with a 20x objective (Plan-Apochromat 20x/0.8 Ph2, Carl Zeiss Sas) with the Zeiss Axio Observer 7 microscope. For quantitative analysis, at least 50 cells per condition distributed over the whole surface were imaged.

2.8 Image analysis, homogeneity analysis and custom-made macros

All images were analyzed with ImageJ [56]. To quantify the cell number, nuclei were identified in each image via this software's Analyze Particles function. The cell number after rinsing was divided by the total cell number before rinsing to obtain a percentage of adherent cells.

Cell area was analyzed by measuring the actin positive area with Analyze Particles (Image J) [56]. The total area of all cells in 1 image was divided by the total number of nuclei, counted as described above, to reduce the influence of overlapping cells [57].

Fluorescently labeled p-SMAD1/5/9 was quantified by measuring its fluorescence intensity inside the nucleus [54, 55]. For this, the nucleus was again identified via the DAPI signal using Analyze Particles (ImageJ) which served as a virtual mask. Then, the intensity of the grey levels of the p-SMAD1/5/9 signal which lie under this mask was extracted and the average background signal was subtracted.

β_1- and β_3-integrins were only analyzed qualitatively to assess whether or not focal adhesions were formed, and to detect general distribution of integrins in the cell.

The homogeneity of SAv and cRAD, as an example for the binding of biotinylated molecules to SAv, was studied *via* the binding of bATTO to the free biotin binding sites of SAv. After functionalization with bATTO, the surfaces were flipped and put on a microscopy coverslip with an oil-based anti-fade in between. Images were taken with the 63x oil-immersed lens (Plan-Apochromat 63x/1,4 Oil DIC) of a Zeiss LSM 700 confocal microscope (Carl Zeiss Sas) on four different positions per condition and average intensity values were compared to each other.

2.9 Protein isolation and western blot analysis

Approximately 200 000 serum-starved cells were lysed in RIPA buffer (Sigma Aldrich) after 1h for p-SMAD1/5/9 or after 1 h, 24 h or 3 days for integrin quantification as previously reported [28]. Gels were loaded with 500 to 750 ng of protein (25 µg/ml) which was quantified with micro BCA™ assay kit (Thermo Fisher). Blocked membranes were probed with rabbit anti-p-SMAD1/5/9 (1:1000, Cell Signaling Technology), rabbit anti-β_1 (1:2000, produced at the laboratory of Dr Albiges-Rizo, IAB, Grenoble, France) or rat anti-β_3 (1:1000, Luc-A5, Emfret Analytics) together with rabbit anti-GAPDH (1:1000, Cell Signaling Technology) as a reference, all incubated in 1% BSA overnight. Incubation with goat anti-rabbit HRP-conjugated IgG (1:5000 Cell Signaling) and goat anti-rat HRP-conjugated IgG (1:2000 Cell Signaling) was followed by detection with the ChemiDoc Imaging system (Bio-Rad, Hercules, USA) using Clarity or Clarity Maw Western ECL Substrate (Bio-Rad).

2.10 RNA extraction and quantitative polymerase chain reaction (qPCR)

Approximately 200 000 cells were cultured for 24 h before lyse with 350 µL lysis buffer (Machery-Nagel, Dueren, Germany). 4 h after plating, the FBS concentration in the cell media was raised from 0% to 2%. RNA was extracted using the NucleoSpin RNA Plus kit (Macherey-Nagel) according to the manufacturer's protocol, and quantified with UV-Spectrophotometry (Nanodrop 2000, Thermo Fisher Scientific). cDNA transcription and qPCR were carried out using the CFX96 Real-Time system thermo cycler (Bio-Rad) and the corresponding

consumables (Biorad) and primers (Sigma-Aldrich). The Cq values of the target genes were normalized to the reference genes (GUSB, PPIA, Ef1) using the delta-delta-Ct-method [58].

2.11 Alkaline phosphatase (ALP) staining

96-well plates with glued functionalized biomimetic platforms were used for ALP staining. 20 000 cells were plated for each well for 3 days in growth media, with 2% FBS, and fixed in 4% PFA. To quantify total cell number, DAPI staining was performed before ALP staining. To stain ALP, we used fast blue RR salt in a 0.01 % (w/v) naphthol AS-MX solution (Sigma Aldrich) according to the manufacturer's instructions. ALP staining was quantified in dry conditions by scanning the 96-well plate with a scanner (V600 photo, EPSON, Seiko-Epson Corporation), and gray-scale images were acquired at a resolution of 1200 dpi [57]. The images (8-bit) were analyzed with Image J. A threshold of gray was fixed for all conditions (between 0 and 160) to measure the percentage of ALP-positive area per well. This number was normalized to the number of cells in each condition.

2.12 Statistical analysis

Technical replicates where pulled together by taking the average and standard deviation. To compare independent experiments, the values were normalized to a positive control, the average was calculated and the standard error of the mean was used for the error bars in the figures. Significance between two conditions was tested with the non-parametric Mann-Whitney test and represented in the graphs with * for $p \leq 0.05$ and ** for $p \leq 0.01$.

3. RESULTS

3.1 Increasing cRGD surface concentration enhanced BMP2-mediated SMAD signaling

To investigate the effect of integrin activation on BMP2 signaling we tuned the surface concentration of the integrin-ligand cRGD, bound to biotinylated polyethylene glycol of ~ 3200 Da (b-PEG-RGD here named cRGD), on the SAv platform and stimulated cells with soluble BMP2 (sBMP2) at a constant concentration of 6 nM (**Figure 1a**).

Before performing cellular experiments, we characterized the binding of cRGD to SAv with a combined QCM-D and SE setup (**Figure 1b**). The black curve in **Figure 1b** is a spectroscopic ellipsometry dynamic fitting of the Δ and Ψ ellipsometric angles obtained during the adsorption of cRGD on SAv at a 0.25 μM soluble concentration. At equilibrium, 22.6 ± 1.2 ng/cm^2 of cRGD were bound to the SAv monolayer. To reduce the surface amount of cRGD, its adsorption was stopped at 1 and 3 minutes, generating an adsorbed mass of 2.1 ± 0.1 and 10.1 ± 1.0 ng/cm^2 respectively. Considering a homogenous coating of cRGD molecules on the SAv monolayer (as shown in **Figure SI1**) and an average molecular weight of the peptide of 3.9 kDa, we calculated

that these values correspond to an intra-molecular distance of ~ 17, 8 and 5 nm for the 1, 3 minutes and saturated cRGD, respectively.

C2C12 cells were plated on these cRGD platforms and after 1 hour of stimulation with sBMP2, the cells were lysed for Western blot analysis. As a positive control, C2C12 cells were plated on plastic Petri dishes (TCPS) and stimulated with the same concentration of sBMP2. **Figures 1c** and **1d** show that SMAD1/5/9 phosphorylation was upregulated in cells plated on higher cRGD surface concentrations (23 ng/cm^2) compared to lower cRGD surface concentrations (2 ng/cm^2). These results indicate that SMAD1/5/9 phosphorylation is cRGD dose-dependent. Increasing integrin recruitment at the cell membrane therefore enhances BMP2 bioactivity.

To further prove that this effect is integrin-mediated we replaced cRGD with cRAD peptide (**Figure 1a**). QCM-D measurements (**Figure 1e)** show the binding of three different surface concentrations of cRAD. For that, cRAD adsorption was interrupted before saturation to obtain a sub-monolayer surface density. With a SE and QCM-D combined setup, we quantified the adsorbed amount of cRAD ($\Delta\Gamma$ in ng/cm^2) relative to the frequency shift (Δf in Hz) measured with the QCM-D (**Figure 1f)**. This curve makes it possible to deduce the optical mass from shifts in frequency and leads to calculated surface concentrations of 19.4 ± 1.1 ng/cm^2 for the saturated cRAD and 9.3 ± 0.7 and 5.4 ± 0.5 ng/cm^2 for the partial cRAD coatings. Homogeneous binding of cRAD on SAv (which was exemplary for biotinylated molecules such as cRGD and bPEG) was measured *via* immunofluorescence using bATTO-565 (**Figure SI1**). As before, C2C12 were plated on cRAD platforms, TCPS and stimulated with sBMP2. On these conditions the increasing surface concentration of cRAD peptide did not improve the cellular p-SMAD1/5/9 response to sBMP2 (**Figure 1g, h**) compared to the cRGD platforms (**Figure 1c**) and TCPS conditions. In **Figure SI2a** we directly compared the effect of cRGD *VS* cRAD peptides with sBMP2 on BMP-SMAD signaling. We demonstrated that p-SMAD1/5/9 levels are significantly lower on cRAD platforms.

However, we observed a basal SMAD1/5/9 phosphorylation in conditions without exogenous integrin ligands which was maybe induced by fibronectin. A previous study from our group has shown that C2C12 cells silenced for fibronectin adhered less to low adhesive surfaces than the scrambled control [43]. We hypothesize that this residual fibronectin, likely secreted while cells were pre-cultured in plastic flasks prior to seeding onto the biomimetic platforms, is recognized by some integrins which may induce basal pSMAD1/5/9 levels on cRAD platforms. The ratio of the normalized levels of p-SMAD1/5/9 of cRGD/cRAD at different peptide concentrations (**Figures 1d** and **1h**, respectively) is plotted in **Figure SI2b**, confirming an increase on higher cRGD surface densities.

These results indicate that BMP2 bioactivity was enhanced by cRGD density, probably through increased engagement of integrins at the cell membrane.

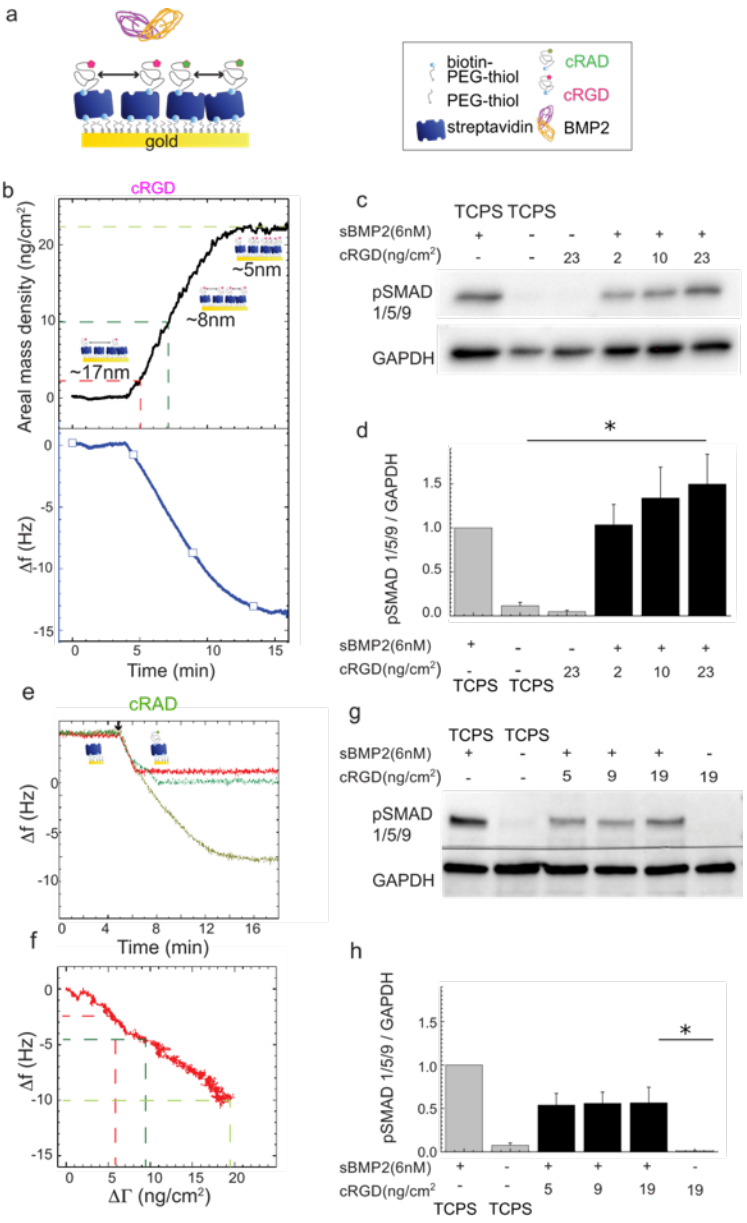

Figure 1: Increasing the surface concentration of cRGD enhances cell response to sBMP2.

a) Schematic representation of the cRGD and cRAD platforms with variable inter-molecular distances between biotinylated peptides. **b**) Combined QCM-D / SE measurement of cRGD binding to SAv. The black curve corresponds to the SE data and the blue curve to the QCM-D binding of cRGD to SAv. The dashed lines mark the incubation times used to functionalize the platforms and the corresponding adsorbed masses. **c**) Western blot of p-SMAD1/5/9 levels in C2C12 cells plated on surfaces presenting three different cRGD surface concentrations and stimulated with sBMP2 (6 nM). As the internal control, C2C12 cells were plated on TCPS with sBMP2. One hour after plating, the cells were lysed and the level of p-SMAD1/5/9 plotted and normalized to the housekeeping gene GAPDH. **d**) Quantification of the Western blot bands. The TCPS control is shown in light grey. The triplicate experiments are available online (http://dx.doi.org/10.17632/p6d4m9gprw.2) **e)** QCM-D measurement showing the adsorption of cRAD at three different incubation times. **f**) $\Delta\Gamma/\Delta f$ calibration curve obtained thanks to a combined SE-QCM-D setup to quantify the quantity of cRAD ($\Delta\Gamma$ ng/cm^2) adsorbed, measured with SE relative to the frequency shift (Δf Hz) measured with the QCM-D. **g**) Western blot of p-SMAD1/5/9 expression on the cRAD platform and its quantification (**h)** as in panel c and d. The triplicate experiments are available online (http://dx.doi.org/10.17632/p6d4m9gprw.2). Bars correspond to the mean ± SEM. The non-parametric Mann-Whitney test was used for single comparisons. *p < 0.05.

3.2 BMP2 improves cell adhesion on low-adhesive platforms

To study the effect of BMP2 on integrin signaling, cell adhesion was considered to be a relevant readout of integrin activation. Previously, BMP2-mediated cell adhesion was demonstrated with soft layer-by-layer biomimetic films presenting matrix-bound BMP2 [43]. Here, we designed low adhesive cRGD platforms with

molecular distances of less than 73 nm, previously shown to be the threshold for cellular adhesion of mesenchymal cells [59, 60]. To do so, simply decreasing the incubation time of cRGD for less than a minute (see **Figure 1b**) may cause experimental errors. We therefore diluted the cRGD peptide in the solution with the inert biotinylated polyethylene glycol (iPEG) molecule (~ 3000 Da) **(Figure SI1a).** After synchronizing their binding kinetics, the cRGD molecular distance could be controlled by different mixtures of both molecules (**Figure SI1b**), while maintaining the sub-monolayer surface density constant, indispensable for other biotinylated molecules to bind.

To compare the effect of soluble *vs* immobilized BMP2 (iBMP2), platforms presenting a cRGD/iPEG mixture were co-functionalized with iBMP2 and characterized with combined QCM-D and SE measurements (**Figure 2a** and **b**, respectively). To this end, the adsorption of the mixture cRGD/iPEG was stopped after 3 minutes of incubation, obtaining total adsorption of 10 ± 1 ng/cm^2 (**Figure 2b** min 38–41). In the case of 10% of cRGD and 90% of iPEG, we expected that 1.0 ± 0.1 ng/cm^2 of cRGD would be immobilized. Assuming a homogeneous distribution of cRGD and iPEG molecules on the SAv monolayer, this surface concentration corresponded to an average distance of 25.5 ± 1.3 nm between cRGD peptides. To further increase this inter-molecular distance, 5%, 2.5% and 1% of cRGD was mixed with 95%, 97.5% and 99% of iPEG resulting in lateral distances of about 36, 51 and 81 nm, respectively (see **Table 2**). iBMP2 was sequentially immobilized on to free-biotin pockets left on the SAv monolayer, generating a frequency shift of -4.3 ± 0.2 Hz, corresponding to a mass of 24.5 ± 0.5 ng/cm^2 (**Figure 2b** min 46–66 and **Table 2**).

Table 2: Surface concentration for each component of the biomimetic surfaces and root-mean-square anchor distances for each component. The polymeric components such as iHS and cRGD are polydisperse and we therefore assumed that the molecular mass of surface-bound molecules is identical to the average molecular weight of the components in solution [25, 26]. Data were obtained from SE measurements. Mean values and standard errors are presented (n=3)

Compound	*Areal mass density (ng cm^{-2})*	*Distance (nm)*
SAv	204.9 ± 9.9	6.9 ± 0.2
+ cRGD	1.0 ± 0.1	25.5 ± 1.3
	0.5 ± 0.1	36.1 ± 1.8
	0.25 ± 0.02	51.1 ± 2.6
	0.10 ± 0.01	80.8 ± 4.1
+ iBMP2	24.5 ± 0.5	13.3 ± 0.1
(after rinsing)	22.3 ± 0.5	13.9 ± 0.2
+ iHS	14.4 ± 0.5	11.9 ± 0.2
+ aBMP2	29.8 ± 1.1	12.1 ± 0.2
(after rinsing)	11.8 ± 1.2	19.2 ± 1.0

C2C12 cells were plated on these platforms and after 1 hour they adhered and, after 1.5 h, they formed integrin β_3 clusters, clearly detectable with confocal microscopy, on cRGD 1 ng/cm^2 but less detectable on lower cRGD

surface concentrations, where C2C12 cells became smaller and punctate (**Figure 2c** and **Figure SI4**). ENCODE studies show that β_1 integrins are more expressed on C2C12 cells than β_3 integrins [61]. On cRGD platforms they were distributed over the entire cell membrane and small β_1 clusters were visible at the cell periphery (**Figure SI4**).

The number of cells that remained adherent to the platforms 1 hour after plating followed by manual rinsing decreased with the reduction of cRGD surface concentration (**Figure 2d**). Only ~10% of cells adhered on platforms with cRGD 0.1 ng/cm^2. Surprisingly, whereas the density of 0.25 ng/cm^2 cRGD was at the limit for inducing cell adhesion, the presence at this concentration of sBMP2 or iBMP2 significantly increased the number of adherent cells (from 30.1 ± 4.1% on cRGD peptide alone to 55.6 ± 6.7 and 66.1 ± 6.5% on sBMP2 and iBMP2, respectively) (**Figure 2d**). For later differentiation studies, it is important to note that the cell area remained unchanged regardless of the type of BMP2 presentation and cRGD surface density (**Figure 2d**). The effect of the same platforms on the adhesion of human periosteum derived stem cells (hPDSCs) was studied. These cells adhered after only 2 hours on cRGD platforms. hPDSCs adhesion decreased on lower cRGD surface concentrations, as for C2C12 cells. However, cellular adhesion was not improved by the presence of BMP2 (**Figure SI5**), likely due to hPDSCs cell ability to secrete BMP2 which can mask the effect of surface-presented BMP2 [62]. On the contrary, our group has previously shown that C2C12 cells do not secrete endogenous BMP2 [21]. hPDSCs became round on 0.1 ng/cm^2, confirming that at an inter-molecular distance of 80 nm, cRGD ligands were too far away to permit cellular spreading.

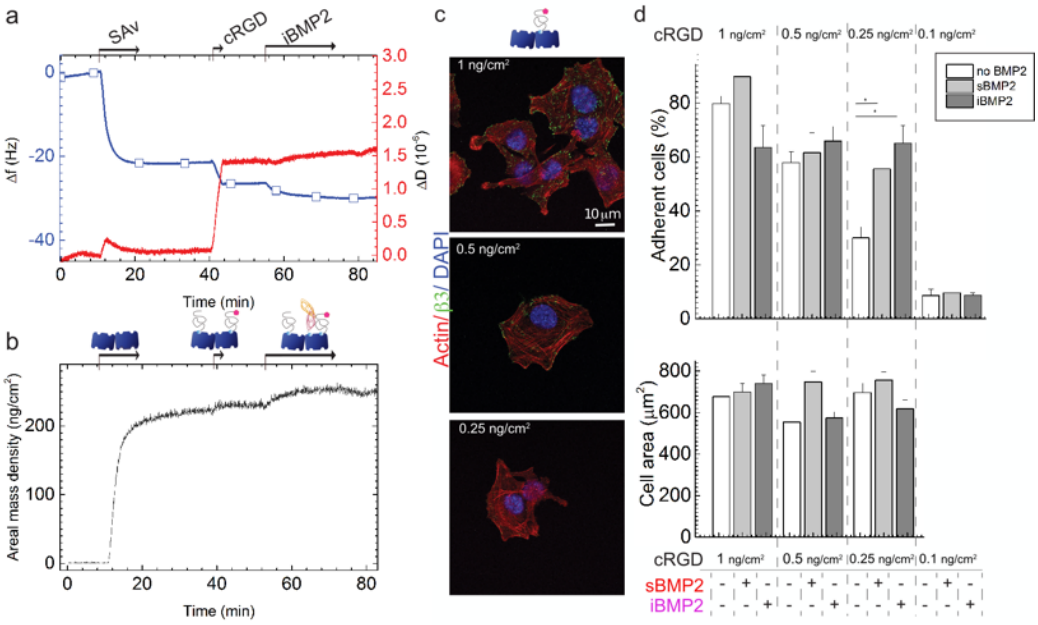

Figure 2: BMP2 improves the number of adherent cells on platforms presenting a 0.25 ng/cm^2 cRGD surface concentration.

a) QCM-D measurement shows the co-functionalization of SAv platforms with cRGD and iBMP2. The blue line shows frequency shifts and the red line dissipation shifts. Arrows indicate the start and duration of the injections. In the remaining time, the surfaces were exposed to running buffer. **b**) SE measurement of mass adsorption. **c)** Confocal immunofluorescence images of C2C12 cells plated on biomimetic platforms presenting different cRGD surface concentrations (from 1 to 0.25 ng/cm^2) and fixed 1.5 hours after seeding. Immunofluorescence staining was performed to reveal the presence of FAs positive for β_3 integrins (labelled in green). Scale bar = 10 μm **d**) Adherent cells remained on the platforms after rinsing and cell area 1 hour after plating. The analysis of cell area was not carried out on 0.1 ng/cm^2 as only a residual number of cells remained adherent to the platforms. Bars correspond to the average value ± standard deviation. A non-parametric Mann-Whitney test was used for single comparisons. *p < 0.05.

We found a threshold value for cRGD surface concentrations (0.25 ng/cm^2) where C2C12 cell adhesion was improved by the presence of sBMP2 and iBMP2. By means of simple and well-defined surface functionalization we directly proved that integrin activation by cRGD ligands improved BMP2-mediated SMAD signaling and that soluble and immobilized BMP2 enhanced C2C12 adhesion.

3.3 C2C12 cell adhesion on cRGD platforms depends on β_3 integrin

We next investigated the involvement of integrins in the synergic signaling observed on cRGD platforms by knocking down either β_1 or β_3 integrins.

First, SAv platforms were engineered to have a comparable amount of cRGD and cRAD, just enough to allow adhesion of a sufficient number of cells to make biomolecular studies possible on both platforms. The concentration in solution of both peptides was adapted to obtain the same binding kinetics measured with QCM-D (**Figure 3a)**. After 4 minutes of incubation, the areal mass densities, deduced from the calibration curves shown in **Figures 1b** and **1f**, of cRGD and cRAD were approximately 8.1 ± 1.2 ng/cm^2 and 7.2 ± 0.5 ng/cm^2, respectively. In this experiment, a significantly higher cRGD surface concentration was used with respect to **Figure 2**.

We observed that C2C12 cells adhered significantly less on cRAD platforms (17.9 ± 7.6%) compared to cRGD platforms (86.5 ± 4.5%) (**Figure 3b)**. The presence of sBMP2 and iBMP2 did not significantly improve cellular adhesion at short time points on cRAD platforms (20.6 ± 6.8% on sBMP2 and 31.7 ± 5.8% on iBMP2), in contrast to the cRGD platforms previously presented (**Figure 2d**).

To investigate whether adhesion on the biomimetic platforms was mediated *via* β_3 or β_1 integrins, both ligands for cRGD, we silenced either one or the other as proved in **Figure 3c**. The silencing of β_1 integrin triggered a small compensation of β_3 integrin [63] at 1 hour after plating (**Figure 3c).**

Wild type (WT) C2C12 cells silenced for β_1 or β_3 integrins (siβ_1 and siβ_3) were plated on the biomimetic platforms presenting cRGD or cRAD ligands with or without sBMP2 (**Figure 3d**). After 1.5 hours on cRGD, WT

cells adhered and spread with an area of about 770 ± 41 μm^2. β_3-integrin silencing generated a significant decrease in cell area (to about 328 ± 9 μm^2), which means that β_3-integrins are crucial for cell spreading on cRGD platforms (**Figure 3d**). β_1-silencing did not affect cell area. The same result was observed in cell adhesion experiments on cRGD platforms (**Figure SI6**). β_3-silenced cells only adhered very moderately on cRGD platforms (11 ± 2%) while silencing β_1 integrin did not affect the number of adherent cells. We observed that the area of cells knocked down for β_1 integrins was slightly, but consistently, larger on cRGD platforms with respect to WT cells. This may be explained by the upregulation of β_3 integrins in siβ_1 cells observed at 1 h after plating on TCPS (**Figure 3c**). On cRAD platforms, cells were round and their cell area was comparable to that of siβ_3 cells. Silencing β_1 or β_3 integrins did not further decrease cell area. All these results indicate that cell adhesion on cRAD platforms was integrin-independent. Furthermore, sBMP2 did not have a significant effect on the area of integrin silenced cells (**Figure 3d**), which is probably due to the efficient down-regulation of β_3 integrins compared to their reduced engagement *via* low cRGD concentration as seen in **Figure 2d**.

C2C12 cells adhered to cRGD platforms mainly via β_3 integrins. No other integrins have been studied, so far, since cRGD ligands are known to be specific for these two types of integrins [46]. In addition, cell adhesion on cRAD peptides is negligible, even in the presence of sBMP2, and integrin-independent, showing that cRAD was an appropriate negative control.

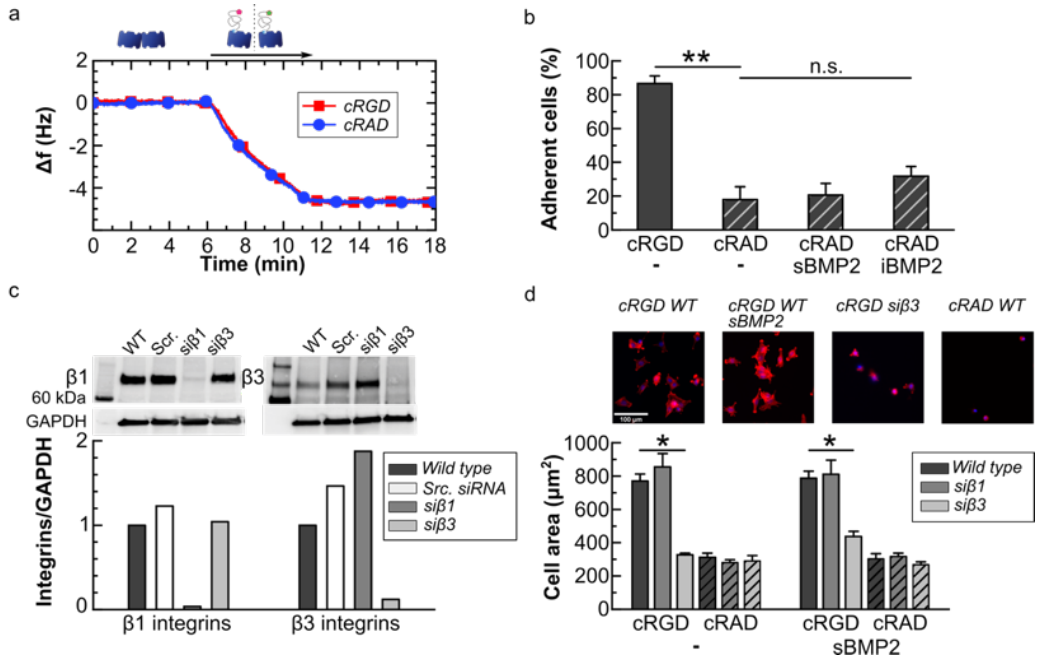

Figure 3: cRGD platforms specifically tune integrin β_3 mediated cell adhesion. a) The QCM-D graph shows the cRGD (red curve) and cRAD (blue curve) binding to the SAv monolayer with the same kinetics. **b)** Ratio of adherent wild type C2C12 cells plated on cRGD and cRAD co-functionalized platforms together with sBMP2 and iBMP2. **c)** Western blot and quantification of wild type, scrambled, β_1 and β_3 silenced cells 1 hour after plating. Expression of integrins was normalized to GAPDH **d)** Cell spreading area on cRGD *VS* cRAD platforms. C2C12 were fixed after 90 min and stained with DAPI (nucleus), phalloidin (F-actin) for fluorescent microscopy. Scale bar = 100 μm. In **b** and **d**, bars represent the

mean of three independent experiments ± SEM. A Mann-Whitney test was used for single comparisons. *$p < 0.05$, **$p < 0.01$, n.s. stands for not statistically significant.

3.4 Extracellular HS stabilizes the BMP2-SMAD1/5/9 signaling pathway independently of cRGD surface concentration without influencing cellular adhesion and spreading.

To better understand the role of the ECM on the BMP2 signaling pathway, we added a degree of complexity to these platforms by studying the effect of heparan sulfate on BMP2-mediated cellular adhesion and differentiation.

To study the combined effect of iHS with cRGD ligands on BMP2 bioactivity, we compared BMP2 adsorbed on iHS (aBMP2) to sBMP2 and iBMP2 on different cRGD surface concentrations. Biomimetic platforms presenting iHS were engineered and characterized with QCM-D and SE (**Figure 4a,b**). The surface amount of cRGD was reduced from 1.00 to 0.25 ng/cm^2, as before in **Figure 2**, by maintaining the same amount of immobilized HS (iHS). iHS was grafted on SAv with a mass density of 14.4 ± 0.5 ng/cm^2. On iHS, 29.8 ± 1.1 ng/cm^2 of BMP2 was adsorbed. It is important to note (**Table 2**) that the amount of aBMP2 adsorbed to iHS was comparable to the amount of iBMP2 adsorbed on SAv platforms, as previously characterized **(Figure 2a,b**). After rinsing with Hepes buffer, part of the aBMP2 was removed, confirming the partially reversible binding between HS and BMP2 [28]. The addition of DMEM during the BMP2 rinsing, accelerated the partial (~ 50%) desorption of BMP2, which reached its equilibrium after few minutes (**Figure SI7**).

To study the effect of iHS on aBMP2 bioactivity on different cRGD surface concentrations, we plated C2C12 cells for 1 hour on cRGD platforms with sBMP2, iHS, iHS + aBMP2 and iBMP2 (**Figure 4c**). We analyzed the phosphorylation of SMAD1/5/9 using Western blot. First, we observed that the level of p-SMAD1/5/9 significantly decreased with the decreasing cRGD surface concentrations in the case of both sBMP2 and iBMP2. Platforms functionalized with iHS + aBMP2 maintained constant levels of p-SMAD1/5/9 even at low cRGD surface concentrations (**Figure 4c**).

It is worth noting that SMAD1/5/9 phosphorylation was sustained on iHS + aBMP2 during the first 6 hours after plating, while this signaling decreased with time on both sBMP2 and iBMP2 (**Figure SI8a**).

Cellular adhesion on 0.25 ng/cm^2 of cRGD, was not improved by iHS alone, but by the presence of iHS + aBMP2 **(Figure SI9b)**.

The effect of HS on BMP2 bioactivity was also studied on hPDSCs at a later time point (2 hours), due to the slower cellular adhesion to the platforms compared to C2C12 cells (**Figure SI9c,d**). A cRGD surface concentration of 0.5 ng/cm^2 was used to obtain a sufficient quantity (75 ± 3%) of cells adhered on the platforms (**Figures SI5a and SI9d**). The levels of p-SMAD1/5/9 were analyzed using Western blot, and the highest levels

of p-SMAD1/5/9 were observed on iHS + aBMP2 platforms, condition that significantly upregulated SMAD1/5/9 phosphorylation with respect to the iHS alone (**Figure 4d**).

We proved with two different cell models that iHS had a positive influence on BMP2 bioactivity. For C2C12 cells, it stabilized and sustained the p-SMAD1/5/9 levels over time. For hPDSCs iHS + aBMP2, it enhanced SMAD phosphorylation as compared to sBMP2 and iBMP2.

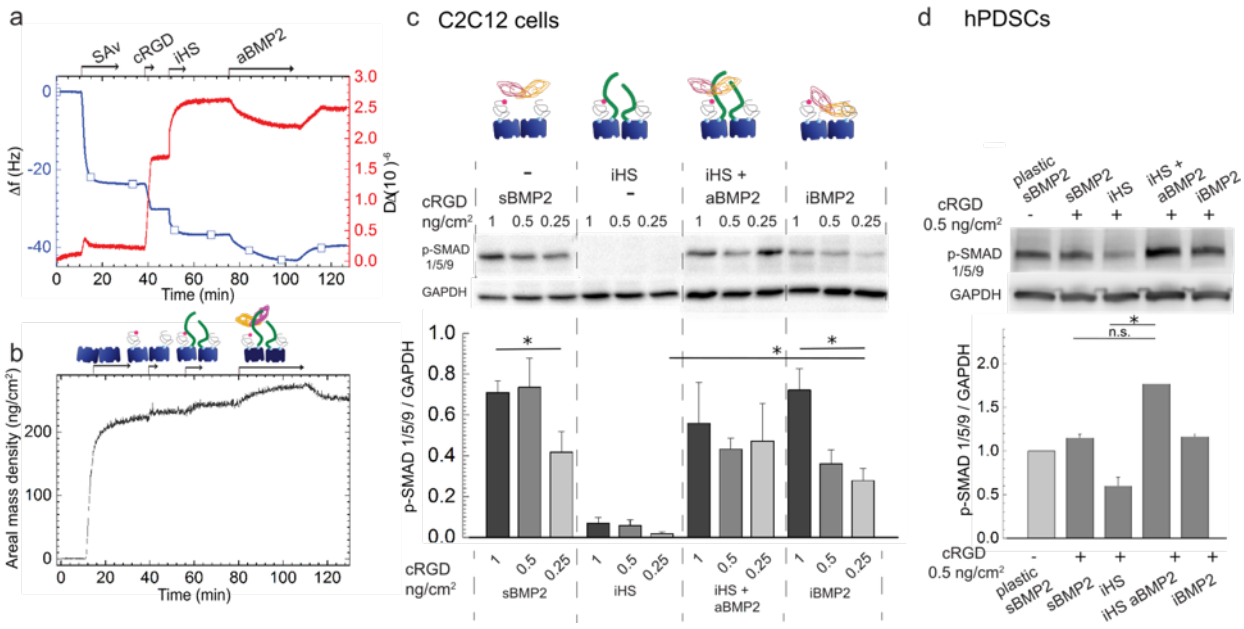

Figure 4: iHS has a positive effect on BMP2-mediated SMAD1/5/9 phosphorylation

a, b) Biomimetic platform characterization using the QCM-D (a) and SE (b) techniques.

c) Western blot and quantification of p-SMAD1/5/9 in C2C12 cells plated on platforms functionalized with different cRGD surface concentrations and with sBMP2, iHS, iHS and aBMP2 and iBMP2. Cells were lysed 1 hour after plating and the phosphorylation of SMAD1/5/9 was normalized to GAPDH (n=4). All the Western blots used for quantification are available online http://dx.doi.org/10.17632/y8mscmkcxk.2

d) Western blot and quantification of p-SMAD1/5/9 after 2h in hPDSCs plated on different platforms presenting sBMP2, iHS, iHS + aBMP2, and iBMP2. Three independent experiments were compared and are available online (DOI: 10.17632/y8mscmkcxk.2). Bars correspond to the mean ± SEM. A Mann-Whitney test was used for single comparisons. **p* < 0.05, n.s. stands for not statistically significant.

3.5 β_3 and β_1 integrins are important for SMAD1/5/9 phosphorylation and ALP expression.

As previous results have shown the cooperation between integrin and BMPRs for driving BMP2 signaling on a BMP2-bound soft matrix [43], we investigated whether integrins play a part in the sustained BMP2 signaling induced by the biomimetic platforms and, if so, which ones. For this purpose, β_1 or β_3 integrins were silenced in the conditions where C2C12 cells were plated on different platforms co-presenting cRGD or cRAD and sBMP2 or iHS or iHS + aBMP2 or iBMP2. BMP2 signaling was analyzed either after 1.5 hours for p-SMAD1/5/9 staining (**Figure 5a**) or after 3 days for ALP staining (**Figure 5c**).

Figure 5b shows quantification of nuclear translocated p-SMAD1/5/9 intensity for each condition and cell type**.** On cRAD platforms the levels of p-SMAD1/5/9 were significantly lower than on cRGD platforms and not further reduced after silencing either β_3 or β_1 integrins. This result is in agreement with the previous Western blot in **Figures 1g and h** showing that cRGD platforms enhanced the phosphorylation of SMAD compared to cRAD platforms. The phosphorylation of SMAD1/5/9 remained low during the 6 hours after BMP2 stimulation on cRAD platforms (**Figure SI10)**.

On cRGD platforms, SMAD1/5/9 phosphorylation was downregulated regardless of whether either β_3 or β_1 integrins were silenced, independently of the type of BMP2 presentation (iHS + aBMP2 *vs* iBMP2), but not down to the levels measured on the cRAD platforms. Both integrins were therefore involved in p-SMAD1/5/9 signaling activation, independently of the presence of iHS.

Silencing β_3 or β_1 integrins also led to downregulated expression of ALP (**Figure 5d)** in particular on cRGD platforms presenting sBMP2 and aBMP2, but this trend was noticeable also on cRAD platforms.

We tested integrin expression 24 h and 3 days after plating, and the levels of silenced integrins remained downregulated (**Figure SI11**), indicating that the silencing was efficient for a long time after transfection.

Surprisingly, after 3 days, C2C12 cells were positive for ALP on both cRGD and cRAD platforms presenting iHS + aBMP2 (**Figures 5c and d**). In particular, iHS + aBMP2 enhanced ALP activity with respect to sBMP2 on cRAD platforms and with respect to iBMP2 on both cRAD and cRGD platforms.

We therefore observed that both integrins, β_3 and β_1, were important for p-SMAD1/5/9 signaling and, later on, for ALP expression. Moreover, cells were able to differentiate on cRAD platforms presenting iHS + aBMP2, even if p-SMAD1/5/9 levels were low during the first 6 hours after plating, probably due to later cellular expression of matrix proteins [64]. Of note is that the presence of iHS + aBMP2 enhanced ALP staining independently of the adhesion ligands. The downregulation of integrins decreased both p-SMAD and ALP on HS + aBMP2 conditions, revealing that both integrins and iHS were fundamental actors in the promotion of the BMP2-mediated signaling pathway.

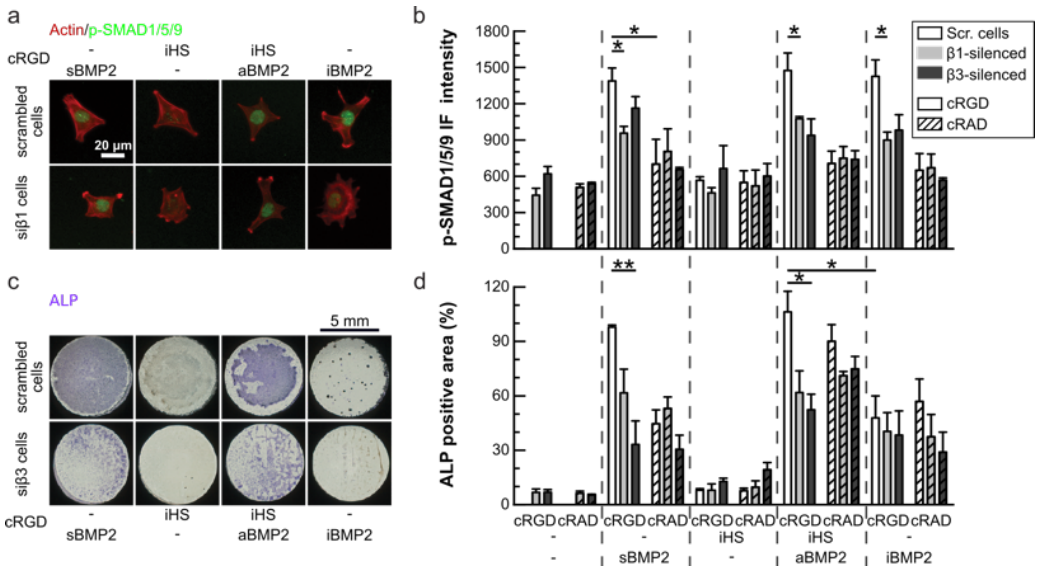

Figure 5: Effect of the ligand (cRAD *vs* cRGD) and the presence of specific integrins on the regulation of the p-SMAD1/5/9 pathway and ALP expression.

Cells were silenced for either β_1 or β_3 integrins and plated on cRGD and cRAD platforms presenting sBMP2, iHS, iHS + aBMP2 and iBMP2, and fixed after 1.5 h for p-SMAD1/5/9 staining (**a**) or after 3 days for ALP staining (**c**). **a)** Representative IF images of scrambled and silenced β_1 (siβ1) cells plated on cRGD platforms and stained for actin (red) and p-SMAD1/5/9 (green). Scale bar = 20 μm. Representative images of all the conditions are available online: http://dx.doi.org/10.17632/ip9m2nmpry.4. In graphics b and d, scrambled cells are represented with white bars, silenced β_1 cells (siβ1) with grey and silenced β_3 cells (siβ3) with dark grey bars. Cells plated on cRAD platforms are represented with patterned bars. Bars represent the mean of three independent experiments ± SEM. **b)** Immunofluorescence intensity of p-SMAD1/5/9 translocated into cell nuclei. Number of quantified cells was >50 for each experiment and condition **c)** Representative wells after ALP staining for scrambled and silenced β_3 (siβ3) cells plated on cRGD platforms. Representative images of all the conditions are available online: http://dx.doi.org/10.17632/ip9m2nmpry.4. **d)** ALP positive area normalized by the number of cells in each well (n=3). Scale bar = 5 mm. A Mann-Whitney test was used for single comparisons. *$p < 0.05$, **$p < 0.01$.

3.6 Immobilized HS enhances BMP2-mediated osteogenic differentiation

To further assess the effect of HS and integrin engagement on BMP2-mediated osteogenic differentiation, expression of osteogenic transcription factors in C2C12 and hPDSCs was analyzed with qPCR. Serum-starved C2C12 cells were plated on biomimetic platforms presenting decreasing cRGD surface concentrations and different types of BMP2 presentations (sBMP2, iHS + aBMP2 and iBMP2). The condition with only iHS was used as the negative control as we had previously proved that iHS alone did not trigger BMP2 activity in either C2C12 or hPDSCs (**Figures 4 c and d** and **Figures 5 b and d**). Expression of the osteogenic markers Osterix and Runx2 was analyzed 24 hours after plating as expression of these markers is detectable after this time period [65]. We observed that neither transcription factor responded to cRGD surface concentrations (**Figures 6a and b**) and they were upregulated on iHS + aBMP2, in particular with low cRGD surface concentrations (**Figures 6a and b**) with respect to the iBMP2 condition.

Expression of the osteogenic transcription factors Osterix and Dlx5 was upregulated on hPDSCs plated for 3 days on biomimetic platforms presenting iHS + aBMP2, while expression of Runx2 and Sox-9 (a chondrogenic marker) was not influenced by the type of BMP2 presentation (**Figure SI12**). Both results proved that iHS has a positive effect on BMP2-mediated osteogenic differentiation.

We also determined expression of Osterix and Runx2 on cRAD platforms in comparison with cRGD platforms presenting the same peptide surface concentration (**Figure 3a**). On cRAD platforms, expression of Osterix and Runx2 was lower than on cRGD platforms **(Figures 6c and d)** but higher than the negative control. Expression of Runx2 and Osterix was upregulated on cRGD and cRAD platforms presenting HS + aBMP2 with respect to the negative control. However, only on cRGD platforms was the osteogenic differentiation by iHS + aBMP2 significantly higher than on iBMP2 (**Figure 6d**).

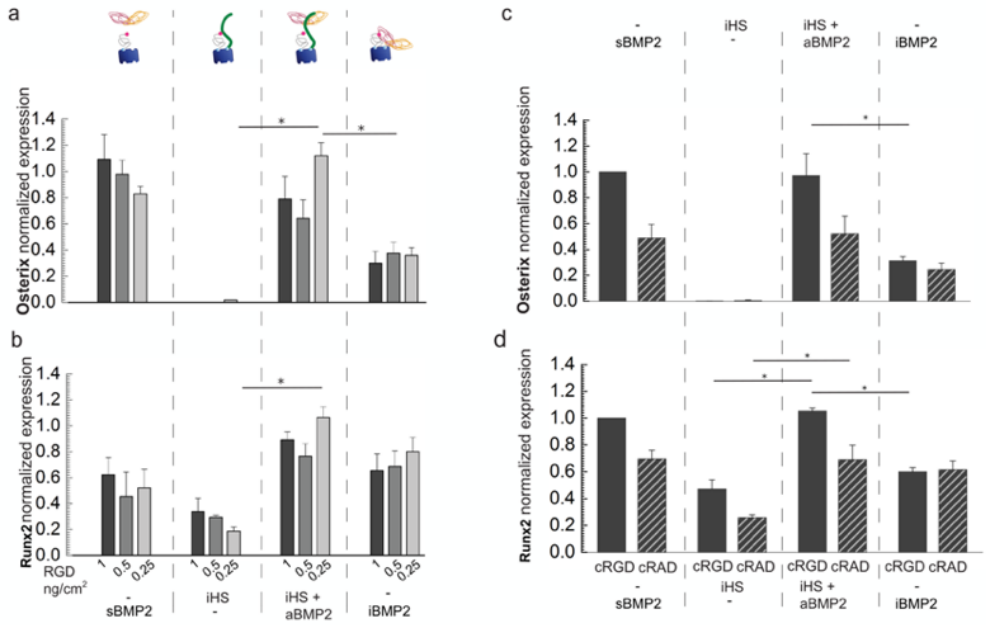

Figure 6: Osteogenic markers are upregulated when aBMP2 is presented by iHS.

a) Osterix normalized expression in C2C12 which differentiated 1 day on platforms functionalized with different cRGD surface concentrations, sBMP2, iHS with or without aBMP2 and iBMP2 (n=5). **b**) Runx2 normalized expression analyzed in parallel to Osterix on the same biomimetic platforms. **c)** Osterix normalized expression of C2C12 cells plated 1 day on platforms with the same amount of cRGD and cRAD and with BMP2 alone or adsorbed to HS. **d)** Runx2 normalized expression quantified in parallel on the same conditions as for Osterix. Bars correspond to the average ± SEM (n=3). A Mann-Whitney test was used for single comparisons. *p < 0.05: **p<0.01.

4 DISCUSSION

We engineered a multivalent substrate to mimic the extracellular matrix and to control the surface density of the adhesion ligands, iHS and BMP2, to provide previously unknown evidence of the effect of integrin adhesion ligands and HS on BMP2-mediated osteogenic differentiation. We shed light on the role of exogenous,

immobilized and oriented HS on BMP2 bioactivity and on its effect on osteogenic differentiation over the course of 72 h.

There are multiple advantages to this biomimetic approach. First, cellular adhesion is specifically controlled by the amount of cRGD peptides immobilized on the platforms. Second, HS and BMP2 are presented homogenously immobilized and adsorbed on the platforms, resembling their state in the ECM. Finally, each molecule has a controlled and reproducible surface density. This biomimetic approach makes it possible to improve the reproducibility of cellular responses and to diminish the artefacts of *in vitro* cell cultures. With respect to our previous studies [25, 26, 28], we proposed innovative SAv-based platforms to (i) tune cellular adhesion (ii) better mimic the ECM *via* the co-presentation of multiple ligands at physiological surface concentrations (cRGD, iHS, aBMP2) (iii) couple receptor silencing with specific ligand presentation (iv) answer fundamental biological questions on the role of ECM components on BMP2-mediated cellular adhesion and osteogenic differentiation, and (v) make long-term cellular studies possible.

Regarding the interplay between cellular adhesion and BMP2 signaling, it is now well-accepted that activation of BMPRs can induce integrin-mediated cell adhesion and migration [39, 43]. Other growth factors, such as hepatocyte growth factor, have been shown to modify β_3 integrin conformation to its active form, thus promoting cell migration [66]. Here, we proved and quantified the bidirectionality of this synergistic effect. Increasing integrin recruitment at the cell membrane by a known amount of cRGD peptides enhanced SMAD1/5/9 phosphorylation in response to sBMP2 (**Figures 1c and d**) and iBMP2 (**Figure 4c**). On the other hand, the presence of sBMP2, iBMP2 and aBMP2 enhanced the number of adherent cells after rinsing at a threshold level for cRGD of 0.25 ng/cm^2 where, without BMP2, only 30% of cells adhered (**Figures 2d** and **SI7a**). Cell area, which is known to regulate BMP2 bioactivity and osteogenesis [67], remained unvaried on platforms presenting different cRGD surface concentrations (**Figures 2d and SI9b)**. On cRGD platforms, C2C12 adhered only *via* β_3 integrins (**Figure 3c**), contrary to what has previously been published by blocking β_3 integrins with soluble peptidomimetic ligands [68].

We observed that increased engagement of β_3 integrins by cRGD peptides induced the peak of SMAD1/5/9 phosphorylation, as compared to the low and stable levels of p-SMAD1/5/9 on cRAD platforms (**Figures 1g and SI2b**). On cRAD platforms, the p-SMAD1/5/9 levels remained significantly lower with respect to the cRGD platforms (**Figures 1 cd-gh,** and **Figure SI2a**).

We observed that BMP2-SMAD signaling and ALP activity were both downregulated on integrin β_1 and in β_3-silenced cells (**Figure 5b**). Thus, on SAv platforms, β_1 integrins were not engaged to improve cellular adhesion but had an effect on SMAD1/5/9 phosphorylation and BMP2-mediated osteogenic differentiation. A

contradictory *in vitro* study revealed that deleting β_1 integrins did not influence p-SMAD1/5 nuclear translocation in osteoblasts, while *in vivo* p-SMAD1/5 signaling was downregulated in the absence of β_1 integrins [69], proving that this regulation might be cell and context-dependent. Of note is the fact that ALP may be influenced by the total number of cells adherent on the platforms and by cell-cell contact that was higher on cRGD platforms presenting BMP2 (soluble, adsorbed and immobilized). We took that aspect into consideration by normalizing the ALP positive area to the total number of cells (**Figure 5d**).

On the biomimetic platforms, downstream BMP2-mediated osteogenic differentiation was enhanced by the presentation of BMP2 *via* immobilized HS. Exogenous HS enhanced BMP2-mediated osteogenic differentiation by sustaining and stabilizing BMP2 bioactivity for longer than sBMP2 and iBMP2 (**Figure SI8**). Surprisingly, iHS+aBMP2 also enhanced ALP staining on cRAD platforms, where p-SMAD1/5/9 was significantly lower. This may be due to activation of the SMAD-independent pathway such as mitogen-activated protein kinase (MAPK), Rho-like GTPase, phosphoinositide 3-kinase (PI3K), as well as c-SRC and LIMK1 signaling and many more [70]. We have tested if the p-p38 pathway was affected by the type of platforms but no differences between cRAD and cRGD platforms were observed (**Figure SI13**). Another hypothesis is that the expression of ALP on cRAD platforms was due to a later secretion of ECM proteins [43, 64] that, after 3 days, may mask the effect of cRAD and cRGD ligands on cell adhesion.

Osteogenic differentiation was lower on immobilized biotinylated BMP2 with respect to aBMP2 (**Figure 5d** and **Figure 6**). The importance of internalization of the BMP2-BMPRs complex is still under debate and has previously been reviewed [18]. Assuming that iBMP2 is not internalized by the cells, our result is in line with previous observations showing that the inhibition of BMP2 endocytosis attenuates osteogenic differentiation [72]. Furthermore, we have previously shown that Noggin may inhibit iBMP2 but not aBMP2 [28]. The low secretion of endogenous Noggin by C2C12 cells and hPDSCs [61] might therefore inhibit the bioactivity of iBMP2, but not of aBMP2. The effect of Noggin inhibition may also explain the kinetics of p-SMAD1/5/9 (**Figure SI8)**, showing that the levels of p-SMAD1/5/9 decreased after the first hour on iBMP2 but not when aBMP2 was presented *via* iHS (**Figure SI8)**. Future studies will clarify the effect of BMP2 antagonists on biomimetic platforms.

This positive effect of iHS on BMP2 signaling and osteogenic differentiation seems in contradiction with developmental studies showing that cell-surface HS inhibits BMP2 bioactivity [31, 73]. We hypothesize that extracellular and cell-surface HS play a different role in BMP2 bioactivity. In line with that, a previous study has reported that the type of HS proteoglycan — present on the cell surface or on the ECM — had a different effect on BMP2-mediated chondrogenic differentiation [74]. In particular, it has been shown that exogenous soluble HS improves BMP-2-mediated chondrogenic differentiation as well as heparitinase treatment of cell-

surface HS-proteoglycans, while the upregulation of Syndecan-3 (cell-surface HS-proteoglycans) suppresses BMP-2-mediated SMAD phosphorylation [74]. To reinforce this hypothesis, further studies with cells presenting no cell-surface HS will be performed. Another cause of variability in the results may be the source and type of sulfation pattern presented on the HS polysaccharidic chain [29]. It has been shown that removing N-sulfations from heparin oligosaccharides significantly reduced BMP2 binding and bioactivity [75].

An interesting observation was that the positive effect of iHS on BMP2-mediated osteogenic differentiation is cRGD ligand concentration-independent (**Figures 6a and b**). We hypothesize that BMP2 bound to HS chains has a degree of flexibility that makes possible optimal orientation of the GFs to recognize its receptors (unlike in previous computational modelling), in comparison to the biotinylated form and, on the top of that, a lateral freedom of movement that facilitates the proximity between integrins and BMPRs as represented in (**Figure 7**). iHS may therefore facilitate BMPRs-integrin crosstalk by allowing the formation of BMPR-integrin clusters, even on low cRGD surface concentrations. The BMPR-integrins crosstalk may thus be sustained and enhanced by the presence of iHS + aBMP2.

iHS may be able to maintain BMP2 close to the cell surface for longer to enable BMP2-mediated osteogenic differentiation even on cRAD platforms where the BMP2 bioactivity is initially not upregulated (**Figures 1 g and h, Figure SI2 and Figure SI10)**. This is confirmed by the upregulation of ALP on iHS + aBMP2 on cRAD platforms (**Figure 5d**).

Regarding the role of iHS alone on integrin-mediated cellular adhesion, we proved that exogenous iHS does not improve cell adhesion even if an interaction between integrins $\alpha_5\beta_1$ and also $\alpha_v\beta_3$ and HS has been previously measured with SPR [76]. The apparent affinity of 2.02 μM [76] is probably not enough to induce integrin-mediated cellular adhesion.

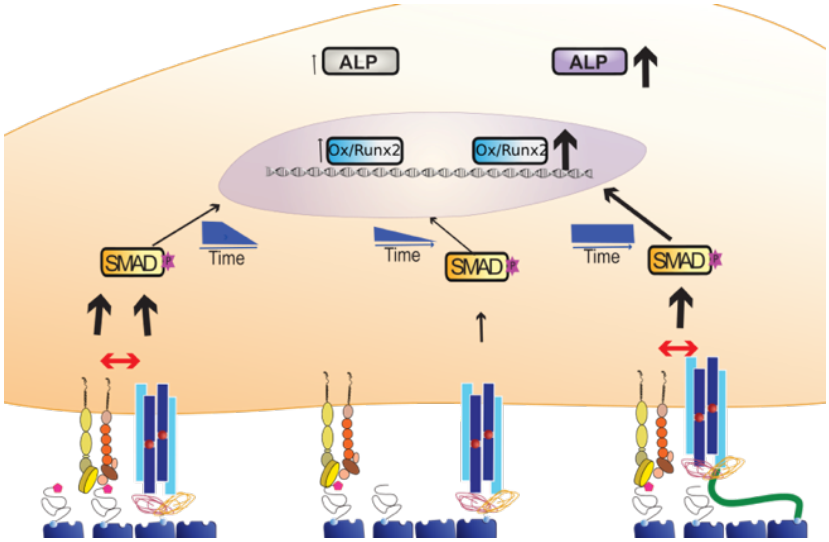

Figure 7: Schematic representation of the effect of integrin-BMPR crosstalk in the presence and absence of HS.

The proximity of BMPRs and integrins, promoted by highly concentrated cRGD ligands, enhances SMAD1/5/9 phosphorylation but only in the first few hours after stimulation. This synergic effect is reduced by decreasing the cRGD surface concentration (central scheme). In the case of iHS + aBMP2 (right side of the image) iHS, being a long molecule, can facilitate the proximity between BMPRs and integrin even in the condition of a low cRGD surface density. Maintaining SMAD phosphorylation for longer, iHS + aBMP2 upregulate the expression of osteogenic markers such as Osterix and Runx2, and promote ALP production.

5 CONCLUSION

Thanks to the controlled functionalization of SAv biomimetic platforms, we revealed the effect of proximity between HS, BMP2 and adhesion ligands on cellular adhesion, BMP2 activity and osteogenic differentiation. While the presentation of exogenous and immobilized HS sustained BMP2-mediated signaling also on platforms which presented low cellular adhesion, its co-immobilization with cRGD peptides optimized BMP2 signaling towards osteogenic differentiation. We also found that both β_1 and β_3 integrins were involved in the upregulation of BMP2-mediated signaling even though cells adhered to the platform only via β_3 integrins. The presence of iHS, however, had no effect on cell adhesion. Moreover, the co-immobilization of cRGD ligands and iHS + aBMP2 upregulated late BMP2-mediated osteogenic differentiation. The adaptable design of the platform makes it a promising candidate for future studies in osteogenic regeneration. Furthermore, positive results on late osteogenic differentiation suggest that biomimetic approaches should be considered for bone repair applications.

6 ACKNOWLEDGMENTS

We would like to acknowledge Prof. Franck Luyten for the donation of hPDSCs, Dr Christian Hiepen, Dr Laure Fourel, Dr Liliane Guerente and Prof. Ralf Richter for the fruitful scientific discussions which inspired some experiments described in this paper. We would like to thank Prof. Joachim Spatz from the Max Planck Institute for Intelligent Systems in Stuttgart (Germany) for his collaboration on the SE measurements. This project received funding from: Fondation Recherche Médicale (No. DEQ20170336746), ANR CODECIDE (No. ANR-17-CE13-022), the European Union's Framework Program for Research and Innovation Horizon 2020 (2014-2020) under the Marie Sklodowska-Curie Grant Agreement No. 658334 and the Initiative de Recherche Stratégique, University Grenoble Alps (IDEX-IRS 2018-2021).

7 REFERENCES

Uncategorized References

[1] A.J. Engler, S. Sen, H.L. Sweeney, D.E. Discher, Matrix elasticity directs stem cell lineage specification, Cell 126(4) (2006) 677-89.
[2] D.E. Discher, D.J. Mooney, P.W. Zandstra, Growth factors, matrices, and forces combine and control stem cells, Science (New York, N.Y.) 324(5935) (2009) 1673-7.
[3] I. Matsuo, C. Kimura-Yoshida, Extracellular distribution of diffusible growth factors controlled by heparan sulfate proteoglycans during mammalian embryogenesis, Philosophical transactions of the Royal Society of London. Series B, Biological sciences 369(1657) (2014).
[4] R.V. Iozzo, L. Schaefer, Proteoglycan form and function: A comprehensive nomenclature of proteoglycans, Matrix biology : journal of the International Society for Matrix Biology 42 (2015) 11-55.
[5] J.R. Bishop, M. Schuksz, J.D. Esko, Heparan sulphate proteoglycans fine-tune mammalian physiology, Nature 446 (2007) 1030.
[6] K. Jochmann, V. Bachvarova, A. Vortkamp, Reprint of: Heparan sulfate as a regulator of endochondral ossification and osteochondroma development, Matrix biology : journal of the International Society for Matrix Biology 35 (2014) 239-47.
[7] M.R. Urist, B.S. Strates, Bone morphogenetic protein, Journal of dental research 50(6) (1971) 1392-406.
[8] F. Liu, A. Hata, J.C. Baker, J. Doody, J. Carcamo, R.M. Harland, J. Massague, A human Mad protein acting as a BMP-regulated transcriptional activator, Nature 381(6583) (1996) 620-3.
[9] G. Rawadi, B. Vayssiere, F. Dunn, R. Baron, S. Roman-Roman, BMP-2 controls alkaline phosphatase expression and osteoblast mineralization by a Wnt autocrine loop, Journal of bone and mineral research : the official journal of the American Society for Bone and Mineral Research 18(10) (2003) 1842-53.
[10] A. Nohe, S. Hassel, M. Ehrlich, F. Neubauer, W. Sebald, Y.I. Henis, P. Knaus, The mode of bone morphogenetic protein (BMP) receptor oligomerization determines different BMP-2 signaling pathways, The Journal of biological chemistry 277(7) (2002) 5330-8.
[11] R. Ruppert, E. Hoffmann, W. Sebald, Human bone morphogenetic protein 2 contains a heparin-binding site which modifies its biological activity, European journal of biochemistry / FEBS 237(1) (1996) 295-302.
[12] J.T. Gallagher, Heparan sulfate: growth control with a restricted sequence menu, J Clin Invest 108(3) (2001) 357-61.
[13] D.S. Bramono, S. Murali, B. Rai, L. Ling, W.T. Poh, Z.X. Lim, G.S. Stein, V. Nurcombe, A.J. van Wijnen, S.M. Cool, Bone marrow-derived heparan sulfate potentiates the osteogenic activity of bone morphogenetic protein-2 (BMP-2), Bone 50(4) (2012) 954-64.
[14] M.M. Martino, J.A. Hubbell, The 12th-14th type III repeats of fibronectin function as a highly promiscuous growth factor-binding domain, FASEB journal : official publication of the Federation of American Societies for Experimental Biology 24(12) (2010) 4711-21.
[15] S.E. Sakiyama-Elbert, Incorporation of heparin into biomaterials, Acta biomaterialia 10(4) (2014) 1581-7.
[16] M.M. Martino, P.S. Briquez, K. Maruyama, J.A. Hubbell, Extracellular matrix-inspired growth factor delivery systems for bone regeneration, Advanced drug delivery reviews 94 (2015) 41-52.
[17] J. Nickel, P. Ten Dijke, T.D. Mueller, TGF-beta family co-receptor function and signaling, Acta biochimica et biophysica Sinica 50(1) (2018) 12-36.
[18] E. Migliorini, A. Valat, C. Picart, E.A. Cavalcanti-Adam, Tuning cellular responses to BMP-2 with material surfaces, Cytokine & growth factor reviews 27 (2016) 43-54.
[19] A.S. Curry, N.W. Pensa, A.M. Barlow, S.L. Bellis, Taking cues from the extracellular matrix to design bone-mimetic regenerative scaffolds, Matrix biology : journal of the International Society for Matrix Biology 52-54 (2016) 397-412.
[20] T. Crouzier, L. Fourel, T. Boudou, C. Albiges-Rizo, C. Picart, Presentation of BMP-2 from a soft biopolymeric film unveils its activity on cell adhesion and migration, Advanced materials (Deerfield Beach, Fla.) 23(12) (2011) H111-8.
[21] T. Crouzier, K. Ren, C. Nicolas, C. Roy, C. Picart, Layer-by-layer films as a biomimetic reservoir for rhBMP-2 delivery: controlled differentiation of myoblasts to osteoblasts, Small (Weinheim an der Bergstrasse, Germany) 5(5) (2009) 598-608.
[22] R. Anouz, A. Repanas, E. Schwarz, T. Groth, Novel Surface Coatings Using Oxidized Glycosaminoglycans as Delivery Systems of Bone Morphogenetic Protein 2 (BMP-2) for Bone Regeneration, Macromolecular bioscience 18(11) (2018) 1800283.

[23] E. Migliorini, D. Thakar, J. Kuhnle, R. Sadir, D.P. Dyer, Y. Li, C. Sun, B.F. Volkman, T.M. Handel, L. Coche-Guerente, D.G. Fernig, H. Lortat-Jacob, R.P. Richter, Cytokines and growth factors cross-link heparan sulfate, Open biology 5(8) (2015).
[24] D. Thakar, E. Migliorini, L. Coche-Guerente, R. Sadir, H. Lortat-Jacob, D. Boturyn, O. Renaudet, P. Labbe, R.P. Richter, A quartz crystal microbalance method to study the terminal functionalization of glycosaminoglycans, Chemical communications (Cambridge, England) 50(96) (2014) 15148-51.
[25] E. Migliorini, D. Thakar, R. Sadir, T. Pleiner, F. Baleux, H. Lortat-Jacob, L. Coche-Guerente, R.P. Richter, Well-defined biomimetic surfaces to characterize glycosaminoglycan-mediated interactions on the molecular, supramolecular and cellular levels, Biomaterials 35(32) (2014) 8903-15.
[26] D. Thakar, F. Dalonneau, E. Migliorini, H. Lortat-Jacob, D. Boturyn, C. Albiges-Rizo, L. Coche-Guerente, C. Picart, R.P. Richter, Binding of the chemokine CXCL12alpha to its natural extracellular matrix ligand heparan sulfate enables myoblast adhesion and facilitates cell motility, Biomaterials 123 (2017) 24-38.
[27] S. Sarrazin, W.C. Lamanna, J.D. Esko, Heparan Sulfate Proteoglycans, Cold Spring Harbor Perspectives in Biology 3(7) (2011).
[28] E. Migliorini, P. Horn, T. Haraszti, S. Wegner, C. Hiepen, P. Knaus, P. Richter, E. Cavalcanti-Adam, Enhanced biological activity of BMP-2 bound to surface-grafted heparan sulfate, Advanced Biosystems 1(4) (2017) 1600041.
[29] S. Murali, B. Rai, C. Dombrowski, J.L. Lee, Z.X. Lim, D.S. Bramono, L. Ling, T. Bell, S. Hinkley, S.S. Nathan, J.H. Hui, H.K. Wong, V. Nurcombe, S.M. Cool, Affinity-selected heparan sulfate for bone repair, Biomaterials 34(22) (2013) 5594-605.
[30] R.A.A. Smith, R.J.E. Chua, S.M. Carnachan, C.L.L. Tan, I.M. Sims, S.F.R. Hinkley, V. Nurcombe, S.M. Cool, Retention of the structure and function of heparan sulfate biomaterials after gamma irradiation, Tissue engineering. Part A (2017).
[31] J. Huegel, M. Enomoto-Iwamoto, F. Sgariglia, E. Koyama, M. Pacifici, Heparanase stimulates chondrogenesis and is up-regulated in human ectopic cartilage: a mechanism possibly involved in hereditary multiple exostoses, The American journal of pathology 185(6) (2015) 1676-85.
[32] J. Huegel, F. Sgariglia, M. Enomoto-Iwamoto, E. Koyama, J.P. Dormans, M. Pacifici, Heparan sulfate in skeletal development, growth, and pathology: the case of hereditary multiple exostoses, Developmental dynamics : an official publication of the American Association of Anatomists 242(9) (2013) 1021-32.
[33] M. Pacifici, The pathogenic roles of heparan sulfate deficiency in hereditary multiple exostoses, Matrix biology : journal of the International Society for Matrix Biology (2017).
[34] P.C. Billings, M. Pacifici, Interactions of signaling proteins, growth factors and other proteins with heparan sulfate: mechanisms and mysteries, Connect Tissue Res 56(4) (2015) 272-80.
[35] J. Huegel, C. Mundy, F. Sgariglia, P. Nygren, P.C. Billings, Y. Yamaguchi, E. Koyama, M. Pacifici, Perichondrium phenotype and border function are regulated by Ext1 and heparan sulfate in developing long bones: a mechanism likely deranged in Hereditary Multiple Exostoses, Developmental biology 377(1) (2013) 100-12.
[36] L. Koziel, M. Kunath, O.G. Kelly, A. Vortkamp, Ext1-dependent heparan sulfate regulates the range of Ihh signaling during endochondral ossification, Developmental cell 6(6) (2004) 801-13.
[37] E.J. Carragee, E.L. Hurwitz, B.K. Weiner, A critical review of recombinant human bone morphogenetic protein-2 trials in spinal surgery: emerging safety concerns and lessons learned, The spine journal : official journal of the North American Spine Society 11(6) (2011) 471-91.
[38] J. Ivaska, J. Heino, Cooperation between integrins and growth factor receptors in signaling and endocytosis, Annual review of cell and developmental biology 27 (2011) 291-320.
[39] A.I. Monteiro, T. Kollmetz, J. Malmstrom, Engineered systems to study the synergistic signaling between integrin-mediated mechanotransduction and growth factors (Review), Biointerphases 13(6) (2018) 06d302.
[40] A. Sawala, M. Scarcia, C. Sutcliffe, S.G. Wilcockson, H.L. Ashe, Peak BMP responses in the drosophila embryo are dependent on the activation of integrin signaling, Cell reports 12(10) (2015) 1584-93.
[41] A. Shekaran, J.R. Garcia, A.Y. Clark, T.E. Kavanaugh, A.S. Lin, R.E. Guldberg, A.J. Garcia, Bone regeneration using an alpha 2 beta 1 integrin-specific hydrogel as a BMP-2 delivery vehicle, Biomaterials 35(21) (2014) 5453-61.

[42] M. Barczyk, S. Carracedo, D. Gullberg, Integrins, Cell and tissue research 339(1) (2009) 269-280.
[43] L. Fourel, A. Valat, E. Faurobert, R. Guillot, I. Bourrin-Reynard, K. Ren, L. Lafanechere, E. Planus, C. Picart, C. Albiges-Rizo, beta3 integrin-mediated spreading induced by matrix-bound BMP-2 controls Smad signaling in a stiffness-independent manner, The Journal of cell biology 212(6) (2016) 693-706.
[44] J.R. Garcia, A.Y. Clark, A.J. Garcia, Integrin-specific hydrogels functionalized with VEGF for vascularization and bone regeneration of critical-size bone defects, Journal of biomedical materials research. Part A 104(4) (2016) 889-900.
[45] J.E. Frith, R.J. Mills, J.J. Cooper-White, Lateral spacing of adhesion peptides influences human mesenchymal stem cell behaviour, Journal of cell science 125(Pt 2) (2012) 317-27.
[46] M. Pfaff, K. Tangemann, B. Muller, M. Gurrath, G. Muller, H. Kessler, R. Timpl, J. Engel, Selective recognition of cyclic RGD peptides of NMR defined conformation by alpha IIb beta 3, alpha V beta 3, and alpha 5 beta 1 integrins, The Journal of biological chemistry 269(32) (1994) 20233-8.
[47] T. Katagiri, A. Yamaguchi, M. Komaki, E. Abe, N. Takahashi, T. Ikeda, V. Rosen, J.M. Wozney, A. Fujisawa-Sehara, T. Suda, Bone morphogenetic protein-2 converts the differentiation pathway of C2C12 myoblasts into the osteoblast lineage, The Journal of cell biology 127(6 Pt 1) (1994) 1755-66.
[48] J. Bolander, W. Ji, J. Leijten, L.M. Teixeira, V. Bloemen, D. Lambrechts, M. Chaklader, F.P. Luyten, Healing of a large long-bone defect through serum-free In itro priming of human periosteum-derived cells, Stem cell reports 8(3) (2017) 758-772.
[49] B. Mulloy, C. Gee, S.F. Wheeler, R. Wait, E. Gray, T.W. Barrowcliffe, Molecular weight measurements of low molecular weight heparins by gel permeation chromatography, Thrombosis and haemostasis 77(4) (1997) 668-74.
[50] G.V. Dubacheva, T. Curk, B.M. Mognetti, R. Auzely-Velty, D. Frenkel, R.P. Richter, Superselective targeting using multivalent polymers, J Am Chem Soc 136(5) (2014) 1722-5.
[51] R.P. Richter, K.B. Rodenhausen, E.N. B.;, M. Schubert, Coupling spectroscopic ellipsometry and quartz crystal microbalance to study organic films at the solid-liquid interface, Springer, Heidelberg, 2014.
[52] J. Bolander, W. Ji, L. Geris, V. Bloemen, Y.C. Chai, J. Schrooten, F.P. Luyten, The combined mechanism of bone morphogenetic protein- and calcium phosphate-induced skeletal tissue formation by human periosteum derived cells, European cells & materials 31 (2016) 11-25.
[53] W. Ji, G. Kerckhofs, C. Geeroms, M. Marechal, L. Geris, F.P. Luyten, Deciphering the combined effect of bone morphogenetic protein 6 and calcium phosphate on bone formation capacity of periosteum derived cells-based tissue engineering constructs, Acta biomaterialia 80 (2018) 97-107.
[54] V. Fitzpatrick, L. Fourel, O. Destaing, F. Gilde, C. Albiges-Rizo, C. Picart, T. Boudou, Signal mingle: Micropatterns of BMP-2 and fibronectin on soft biopolymeric films regulate myoblast shape and SMAD signaling, Scientific reports 7 (2017) 41479.
[55] F. Gilde, L. Fourel, R. Guillot, I. Pignot-Paintrand, T. Okada, V. Fitzpatrick, T. Boudou, C. Albiges-Rizo, C. Picart, Stiffness-dependent cellular internalization of matrix-bound BMP-2 and its relation to Smad and non-Smad signaling, Acta biomaterialia 46 (2016) 55-67.
[56] J. Schindelin, I. Arganda-Carreras, E. Frise, V. Kaynig, M. Longair, T. Pietzsch, S. Preibisch, C. Rueden, S. Saalfeld, B. Schmid, J.Y. Tinevez, D.J. White, V. Hartenstein, K. Eliceiri, P. Tomancak, A. Cardona, Fiji: an open-source platform for biological-image analysis, Nature methods 9(7) (2012) 676-82.
[57] P. Machillot, C. Quintal, F. Dalonneau, L. Hermant, P. Monnot, K. Matthews, V. Fitzpatrick, J. Liu, I. Pignot-Paintrand, C. Picart, Automated buildup of biomimetic films in cell culture microplates for high-throughput screening of cellular behaviors, Advanced materials (Deerfield Beach, Fla.) 30(27) (2018) e1801097.
[58] J. Hellemans, G. Mortier, A. De Paepe, F. Speleman, J. Vandesompele, qBase relative quantification framework and software for management and automated analysis of real-time quantitative PCR data, Genome biology 8(2) (2007) R19.
[59] M. Arnold, E.A. Cavalcanti-Adam, R. Glass, J. Blummel, W. Eck, M. Kantlehner, H. Kessler, J.P. Spatz, Activation of integrin function by nanopatterned adhesive interfaces, Chemphyschem : a European journal of chemical physics and physical chemistry 5(3) (2004) 383-8.

[60] E.A. Cavalcanti-Adam, D. Aydin, V.C. Hirschfeld-Warneken, J.P. Spatz, Cell adhesion and response to synthetic nanopatterned environments by steering receptor clustering and spatial location, HFSP journal 2(5) (2008) 276-85.
[61] E.P. Consortium, An integrated encyclopedia of DNA elements in the human genome, Nature 489(7414) (2012) 57-74.
[62] Q. Wang, C. Huang, M. Xue, X. Zhang, Expression of endogenous BMP-2 in periosteal progenitor cells is essential for bone healing, Bone 48(3) (2011) 524-32.
[63] A. van der Flier, K. Badu-Nkansah, C.A. Whittaker, D. Crowley, R.T. Bronson, A. Lacy-Hulbert, R.O. Hynes, Endothelial alpha5 and alphav integrins cooperate in remodeling of the vasculature during development, Development (Cambridge, England) 137(14) (2010) 2439-49.
[64] V.A. Perez, Z. Ali, T.P. Alastalo, F. Ikeno, H. Sawada, Y.J. Lai, T. Kleisli, E. Spiekerkoetter, X. Qu, L.H. Rubinos, E. Ashley, M. Amieva, S. Dedhar, M. Rabinovitch, BMP promotes motility and represses growth of smooth muscle cells by activation of tandem Wnt pathways, The Journal of cell biology 192(1) (2011) 171-88.
[65] M.H. Lee, T.G. Kwon, H.S. Park, J.M. Wozney, H.M. Ryoo, BMP-2-induced Osterix expression is mediated by Dlx5 but is independent of Runx2, Biochemical and biophysical research communications 309(3) (2003) 689 - 694.
[66] R. Faccio, M. Grano, S. Colucci, A. Villa, G. Giannelli, V. Quaranta, A. Zallone, Localization and possible role of two different alpha v beta 3 integrin conformations in resting and resorbing osteoclasts, Journal of cell science 115(Pt 14) (2002) 2919-29.
[67] Y.K. Wang, X. Yu, D.M. Cohen, M.A. Wozniak, M.T. Yang, L. Gao, J. Eyckmans, C.S. Chen, Bone morphogenetic protein-2-induced signaling and osteogenesis is regulated by cell shape, RhoA/ROCK, and cytoskeletal tension, Stem cells and development 21(7) (2012) 1176-86.
[68] V. Schaufler, H. Czichos-Medda, V. Hirschfeld-Warnecken, S. Neubauer, F. Rechenmacher, R. Medda, H. Kessler, B. Geiger, J.P. Spatz, E.A. Cavalcanti-Adam, Selective binding and lateral clustering of alpha5beta1 and alphavbeta3 integrins: Unraveling the spatial requirements for cell spreading and focal adhesion assembly, Cell adhesion & migration 10(5) (2016) 505-515.
[69] M. Brunner, N. Mandier, T. Gautier, G. Chevalier, A.S. Ribba, P. Guardiola, M.R. Block, D. Bouvard, beta1 integrins mediate the BMP2 dependent transcriptional control of osteoblast differentiation and osteogenesis, PloS one 13(4) (2018) e0196021.
[70] Y.E. Zhang, Non-Smad Signaling Pathways of the TGF-β Family, Cold Spring Harbor Perspectives in Biology 9(2) (2017).
[71] A. Ulsamer, M.J. Ortuno, S. Ruiz, A.R. Susperregui, N. Osses, J.L. Rosa, F. Ventura, BMP-2 induces Osterix expression through up-regulation of Dlx5 and its phosphorylation by p38, The Journal of biological chemistry 283(7) (2008) 3816-26.
[72] E. Heining, R. Bhushan, P. Paarmann, Y.I. Henis, P. Knaus, Spatial segregation of BMP/Smad signaling affects osteoblast differentiation in C2C12 cells, PloS one 6(10) (2011) e25163.
[73] C. Mundy, E. Yang, H. Takano, P.C. Billings, M. Pacifici, Heparan sulfate antagonism alters bone morphogenetic protein signaling and receptor dynamics, suggesting a mechanism in hereditary multiple exostoses, The Journal of biological chemistry 293(20) (2018) 7703-7716.
[74] M.C. Fisher, Y. Li, M.R. Seghatoleslami, C.N. Dealy, R.A. Kosher, Heparan sulfate proteoglycans including syndecan-3 modulate BMP activity during limb cartilage differentiation, Matrix biology : journal of the International Society for Matrix Biology 25(1) (2006) 27-39.
[75] R.A.A. Smith, S. Murali, B. Rai, X. Lu, Z.X.H. Lim, J.J.L. Lee, V. Nurcombe, S.M. Cool, Minimum structural requirements for BMP-2-binding of heparin oligosaccharides, Biomaterials 184 (2018) 41-55.
[76] C. Faye, C. Moreau, E. Chautard, R. Jetne, N. Fukai, F. Ruggiero, M.J. Humphries, B.R. Olsen, S. Ricard-Blum, Molecular interplay between endostatin, integrins, and heparan sulfate, The Journal of biological chemistry 284(33) (2009) 22029-40.